Highlights

Modeling the Impact of Iron Defect Variability on Silicon Solar Cell Performance Across Different Scenarios

Oleg Olikh,Oleksii Zavhorodnii

- 1
- 2
- 3

Modeling the Impact of Iron Defect Variability on Silicon Solar Cell Performance Across Different Scenarios

Oleg Olikh*, Oleksii Zavhorodnii

Taras Shevchenko National University of Kyiv, 64/13, Volodymyrska Street, Kyiv, 01601, Ukraine

ARTICLE INFO

Keywords:
silicon
iron-boron pairs
solar cells
SCAPS
simulation
defect influence

ABSTRACT

Abstract Abstract

1. Introduction

The necessity for renewable energy sources to meet the growing global demand for sustainable and environmentally friendly energy alternatives has become evident. Among the wide range of renewable energy sources, sunlight is the cleanest, safest, and most abundant source for use in sustainable energy to support economic growth [1]. The utilization of solar energy heavily depends on the use of photovoltaic cells, with silicon–based devices playing a critical role [2, 3].

The issue of semiconductor purity has become increasingly significant since the advent of the transistor in 1947 [4]. The 1960 study by Shockley and Queisser [5] demonstrated that the electrical properties of $n^+ - p$ silicon diodes deteriorate when impurity atoms of metals such as Cu, Fe, Mn, Au, Zn, and Ni are present. This study prompted investigations focused on preventing contaminating metals from entering semiconductors during manufacturing. In particular, metallic impurities are known to reduce the efficiency of silicon–based devices through direct shunting [6], increased leakage current [7], or bulk recombination [8]. Despite extensive study of metallic impurities in silicon over the past fifty years [4, 9], the problem continues to attract significant attention [10, 11, 12, 13, 14].

Iron is prominent among metallic contaminants, with its atoms being among the most prevalent and detrimental impurities in silicon solar cells (SSCs) [15]. Even in small concentrations (about 10^{10} cm^{-3}), point defects related to Fe can significantly influence the performance of SSCs [16, 17]. Therefore, it is of critical importance to assess the concentration of iron impurities. In response to this challenge, various methodologies have been put forward, often based on the property of iron atoms to form pairs with acceptors. In particular, iron atoms are predominantly located in interstitial positions in silicon, forming the Fe_i defect. In *p*–type crystals, without external illumination, iron atoms carry positive charges and tend to bond with negatively charged doping atoms (boron, aluminum, gallium, or indium), forming Fe_iB_{Si} pairs [18]. However, these pairs can destabilized by intense illumination, electron injection, or heating up to 200 °°C [19]. The recombination properties of iron-related defects Fe_i and Fe_iB_s differ significantly, which profoundly affects the overall characteristics of the crystal. This fact formed the basis for the first method of assessing iron concentration [20], which relied on measuring the diffusion length of minority carriers using the surface photovoltage method [21]. Many other methods involve measurements of carrier lifetime [22, 23], Quasi-Steady-State Photoconductance [24], or the study of kinetic dependencies of short-circuit current [25] or photoluminescence intensity [26] during the reaction $Fe_iB_{Si} \rightleftarrows Fe_i + B_{Si}$.

Notably, the presence of Fe–related defects affects the dynamics of electron and hole movement within the solar cell, which is reflected in changes to the appearance of the current–voltage characteristics (I-V) of SSCs overall, as well as modifications to the main photoelectric parameters (short-circuit current I_{SC}, open-circuit voltage V_{OC}, efficiency η, and fill factor FF) in particular. These findings create fundamental possibilities to advance methods for estimating iron concentration by I-V measuring before and after pair dissolution. The advantages of such an approach are associated with the possibility of directly characterizing finished solar cells, as well as the absence of the need for additional equipment other than that required for I-V measurements, which is extremely common. Efforts have been made initially in developing such methods. For instance, it was proposed to estimate the concentration of iron in SSCs

olegolikh@knu.ua (O. Olikh); nevermor464@gmail.com (O. Zavhorodnii)
ORCID(s): 0000-0003-0633-5429 (O. Olikh); 0000-0001-8080-7661 (O. Zavhorodnii)

Table 1
Parameters varied during the simulation

Parameter	Value
d_{p},(μ)	180 – 380
N_{B},(cm^{-3})	$10^{15} - 10^{17}$
N_{Fe},(cm^{-3})	$10^{10} - 10^{14}$
T,(K)	290 – 340
Illumination	AM1.5G, 1000 $\mathrm{W/m^2}$; 940 nm 5 $\mathrm{W/m^2}$; 940 nm 10 $\mathrm{W/m^2}$

based on changes in the ideality factor [27, 28] or open-circuit voltage [17]. However, developing such approaches requires evaluating how a particular parameter changes when iron–containing pairs dissolve and determining whether it can estimate the iron concentration N_{Fe}. For example, the most evident conditions for utilizing a specific parameter include its change due to the transformation $\mathrm{Fe}_i\mathrm{B}_{\mathrm{Si}} \rightarrow \mathrm{Fe}_i + \mathrm{B}_{\mathrm{Si}}$, even by 10 %, along with a monotonic dependence of these changes on N_{Fe}.

This study intends to determine the variations of J_{sc}, V_{oc}, η, and FF resulting from the decay of iron-containing pairs in boron-doped silicon solar cells. Previous similar calculations have been conducted [?], but the results presented in these works typically pertain to particular temperatures, illumination levels (often AM1.5), and solar cells with distinct structures. In this study, we performed calculations over a sufficiently wide temperature range (290-340 K) and for solar cells with varying base thickness (180-380 μ) and doping levels (boron concentration in the base ranging from 10^{15} cm^{-3} to 10^{17} cm^{-3}). The results obtained allow us to assess the feasibility and potential of using the main photovoltaic parameters of specific solar cells to estimate the N_{Fe} value across a range of temperatures, including conditions similar to those encountered in typical SSC applications. Furthermore, investigations have explored changes in photoelectric performance under solar illumination (AM1.5G) and low-intensity monochromatic light (wavelength of 940 nm, intensities of 5 $\mathrm{W/m^2}$ and 10 $\mathrm{W/m^2}$).

In the first case, while it is customary to adhere to standard conditions, it's essential to consider that illumination at 1000 $\mathrm{W/m^2}$ can lead to the disintegration of $\mathrm{Fe}_i\mathrm{B}_s$ complexes. Therefore, measurements for cases requiring the presence of undissociated pairs in silicon must meet specific constraints. On the other hand, intentionally chosen monochromatic illumination penetrates the emitter with negligible losses and does not reach the rear side. In this context, the photoelectric parameters demonstrate a remarkable sensitivity to recombination processes occurring within the solar cell base, making them responsive to variations in iron concentration.

Finally, in our calculations, we attempted to use the latest literature data concerning the exact values of silicon parameters, including light absorption values [?] and coefficients characterizing intrinsic recombination [?].

2. Experimental Methodology

The study involved modeling IV curves of SSCs with an $n^+ - p - p^+$ structure, as illustrated in Figure 1. A notable feature observed in both Al-BSF cells (full area), which are gradually losing relevance, and PERC cells (locally), which are the most widely used in mass production, is the presence of a back surface field (BSF). We considered structures with a base uniformly doped with boron. The doping concentration N_{B}, and the base thickness d_{p} were varied during the modeling process, as detailed in Table 1. The concentration profiles of the dopants, their maximum values ($N^+_{\mathrm{p,max}}$ and $N^+_{\mathrm{n,min}}$), and layer thicknesses (refer to Figure 1) were selected based on the work of Fell et al. [?]

The simulation was conducted using the SCAPS3.3.11 code [?]. SCAPS-1D software, developed by the University of Gent, is founded on theoretical computations that involve solving Poisson's equation, continuity equations for holes and electrons, and drift-diffusion at each position within the solar cell, considering the boundary conditions. Despite its one-dimensional modeling approach, SCAPS is extensively used for modeling various types of solar cells [?] and for investigating the effects of defects on their performance [?].

As can be seen from Table 1, calculations spanned a broad range of temperatures and base doping levels. Therefore, to improve the accuracy of the calculations when inputting the initial parameters into SCAPS, temperature and concentration dependencies (where applicable) of the following silicon parameters were taken into account:

- bandgap according to Passler [29];

- doping induced bandgap narrowing according to to Yan & Cuevas [30];
- effective density of states at conduction and valence band and intrinsic carrier concentration according to Couderc et al. [31];
- thermal carrier velocities according to Green [32];
- free carrier effective masses according to O'Mara et al. [33];
- carrier mobilities according to Klaassen's theory [34];

The values of surface recombination coefficients were considered equal to the thermal velocities of carriers [?]. The calculations addressed recombination processes within the structural volume, incorporating both intrinsic recombination and Shockley-Read-Hall recombination at iron-related defects. In the first case, processes of band-to-band radiation recombination were considered (where the calculation of the corresponding coefficient included the fraction of radiatively emitted photons reabsorbed via band-to-band processes according to Niewelt et al. [?]) and Auger recombination (where the coefficients considered the effect of Coulomb enhancement [?] and temperature dependence [?]).

When accounting for the influence of iron impurities, we considered that Fe atoms were uniformly distributed within the base and p^+ layer, with a total concentration of N_{Fe} (see Table 1). We considered two cases:

Case 1. The concentration of interstitial iron defects $[\mathrm{Fe}_i] = N_{\mathrm{Fe}}$ at each position throughout the solar cell, with no pairs present $[\mathrm{Fe}_i\mathrm{B}_s] = 0$. This case corresponds to the state of the structure immediately after intense illumination, for example.

Case 2. Iron atoms predominantly form pairs with acceptors, $[\mathrm{Fe}_i\mathrm{B}_s] \gg [\mathrm{Fe}_i]$, but the exact concentration ratio depends on the position of the Fermi level and temperature [?] and varies from point to point within the solar cell. Further details about how we calculated the concentration profiles of $\mathrm{Fe}_i\mathrm{B}_s$ and Fe_i are provided in [1]. This case corresponds to prolonged storage of the structure in darkness or under conditions of low-intensity (< 0.01 J/cm^{-3} [?]) illumination.

During the calculations, we assumed that Fe_i forms a single donor level, while the $\mathrm{Fe}_i\mathrm{B}_s$ pair has a trigonal configuration and acts as an amphoteric defect. We obtained defect parameters (including level positions within the bandgap and electron and hole capture cross-sections) from relevant studies [?].

As previously mentioned, we modeled how the solar cell behaves under different illumination conditions, including solar light (AM1.5G) and monochromatic light (wavelength 940 nm, intensities of $\mathrm{W}_{ill} = 5$ W/m^2 or 10 W/m^2) – see Table 1. The calculations incorporated the light absorption values in silicon based on Green's study [Photovoltaics 30 164] [?].

The I-V characteristics were simulated for both Case 1 and Case 2 (see Fig. 2), and from each curve, the short-circuit current density, open-circuit voltage, efficiency, and fill factor were determined. Assessing the influence of iron defect variability relied on the relative changes in each photovoltaic conversion parameter:

$$\epsilon A = \frac{A^{FeB} - A^{Fe}}{A^{FeB}} \times 100\% \tag{1}$$

where A represents one of the parameters (J_{sc}, V_{oc}, FF i η), superscript "FeB" corresponds to the parameter value for coexistence of Fe_i and $\mathrm{Fe}_i\mathrm{B}_s$ (Case 2), superscript "Fe" is related to the decay of all pairs (Case 1).

Impact of change of iron defects was investigated as a function of temperature from 290 K to 340 K, base depth from 180 μ to 380 μ, base doping level from 10^{15} cm^{-3} to 10^{17} cm^{-3}, and total impurity iron atom concentration from 10^{10} cm^{-3} to 10^{14} cm^{-3}. For each illumination scenario, calculations were carried out with 11 different temperature values (T) and 5 base depth values (d_p), evenly distributed within the specified ranges. The concentration values were distributed equally on a logarithmic scale with 4 (N_B case) and 6 (N_{Fe} case) steps per decade. As a result, for the AM1.5 illumination scenario, for instance, 24750 IV characteristics were simulated. An exception occurred with monochromatic illumination at $\mathrm{W}_{ill} = 10$ W/m^2, where we used only two base depth values.

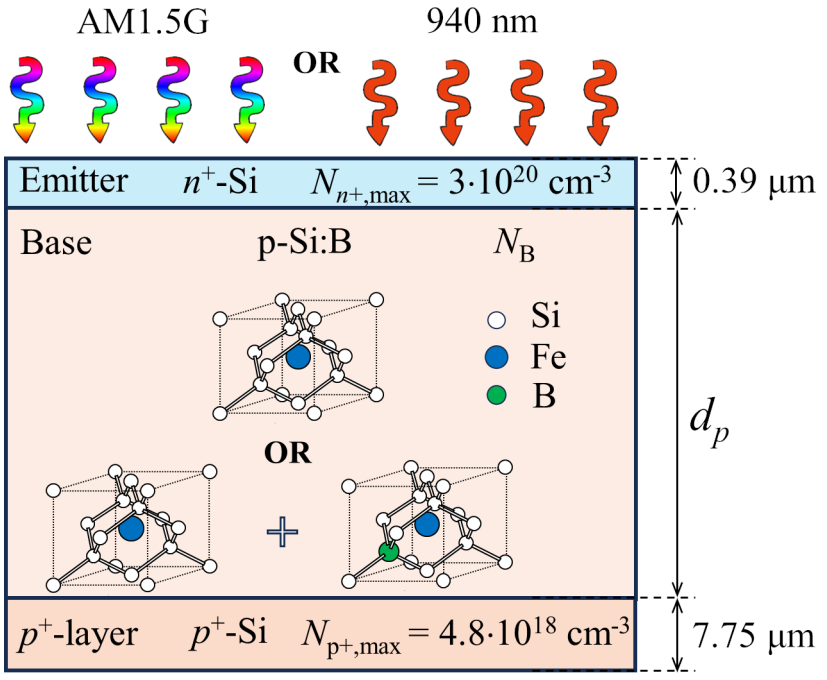

Figure 1: Schematic diagram of analyzed solar cells.

References

[1] B. P. Singh, S. K. Goyal, S. S. A., Grid connected-photovoltaic system (gc-pvs): Issues and challenges, IOP Conference Series: Materials Science and Engineering 594 (2019) 012032.

[2] R. Basnet, D. Yan, D. Kang, M. M. Shehata, P. Phang, T. Truong, J. Bullock, H. Shen, D. Macdonald, Current status and challenges for hole-selective poly-silicon based passivating contacts, Appl. Phys. Rev. 11 (2024) 011311.

[3] L. Wang, J. Liu, Y. Li, G. Wei, Q. Li, Z. Fan, H. Liu, Y. An, C. Liu, J. Li, Y. Fu, Q. Liu, D. He, Dislocations in crystalline silicon solar cells, Advanced Energy and Sustainability Research 5 (2024) 2300240.

[4] C. Claeys, E. Simoen, Metal Impurities in Silicon- and Germanium-Based Technologies: Origin, Characterization, Control, and Device Impact, volume 270 of *Springer Series in Materials Science*, Springer International Publishing, Berlin/New York, 2018.

[5] A. Goetzberger, W. Shockley, Metal Precipitates in Silicon p-n Junctions, J. Appl. Phys. 31 (1960) 1821–1824.

[6] O. Breitenstein, J. P. Rakotoniaina, M. H. Al Rifai, M. Werner, Shunt types in crystalline silicon solar cells, Prog. Photovolt.: Res. Appl. 12 (2004) 529–538.

[7] K. Lee, A. Nussbaum, The influences of traps on the generation-recombination current in silicon diodes, Solid-State Electron. 23 (1980) 655–660.

[8] A. A. Istratov, H. Hieslmair, E. Weber, Iron contamination in silicon technology, Appl. Phys. A 70 (2000) 489–534.

[9] C. W. Pearce, R. G. McMahon, Role of metallic contamination in the formation of "saucer" pit defects in epitaxial silicon, J. Vac. Sci. Technol. 14 (1977) 40–43.

[10] A. Hajjiah, M. Soha, I. Gordon, J. Poortmans, J. John, The impact of interstitial fe contamination on n-type cz-silicon for high efficiency solar cells, Sol. Energ. Mat. Sol. 211 (2020) 110550.

[11] T. T. Le, Z. Zhou, A. Chen, Z. Yang, F. Rougieux, D. Macdonald, A. Liu, Reassessing iron–gallium recombination activity in silicon, J. Appl. Phys. 135 (2024) 133107.

[12] M. Maoudj, D. Bouhafs, N. E. Bourouba, A. Hamida-Ferhat, A. El Amrani, Study of the electrical properties of < 100 > cz p-type solar-grade silicon wafers against the high-temperature processes, Appl. Phys. A 127 (2021) 407.

[13] O. Olikh, O. Datsenko, S. Kondratenko, Influence of illumination spectrum on dissociation kinetics of iron–boron pairs in silicon, Phys. Status Solidi A n/a (2024) 2400351.

[14] H. S. Laine, V. Vähänissi, A. E. Morishige, J. Hofstetter, A. Haarahiltunen, B. Lai, H. Savin, D. P. Fenning, Impact of iron precipitation on phosphorus-implanted silicon solar cells, IEEE Journal of Photovoltaics 6 (2016) 1094–1102.

[15] T. Buonassisi, A. A. Istratov, M. D. Pickett, M. Heuer, J. P. Kalejs, G. Hahn, M. A. Marcus, B. Lai, Z. Cai, S. M. Heald, Chemical natures and distributions of metal impurities in multicrystalline silicon materials, Prog. Photovolt.: Res. Appl. 14 (2006) 513–531.

[16] M. Schubert, M. Padilla, B. Michl, L. Mundt, J. Giesecke, J. Hohl-Ebinger, J. Benick, W. Warta, M. Tajima, A. Ogura, Iron related solar cell instability: Imaging analysis and impact on cell performance, Sol. Energy Mater. Sol. Cells 138 (2015) 96–101.

[17] A. Herguth, Quantification of iron in boron-doped silicon solar cells from open circuit voltage measurements, IEEE J. Photovolt. 12 (2022) 937–947.

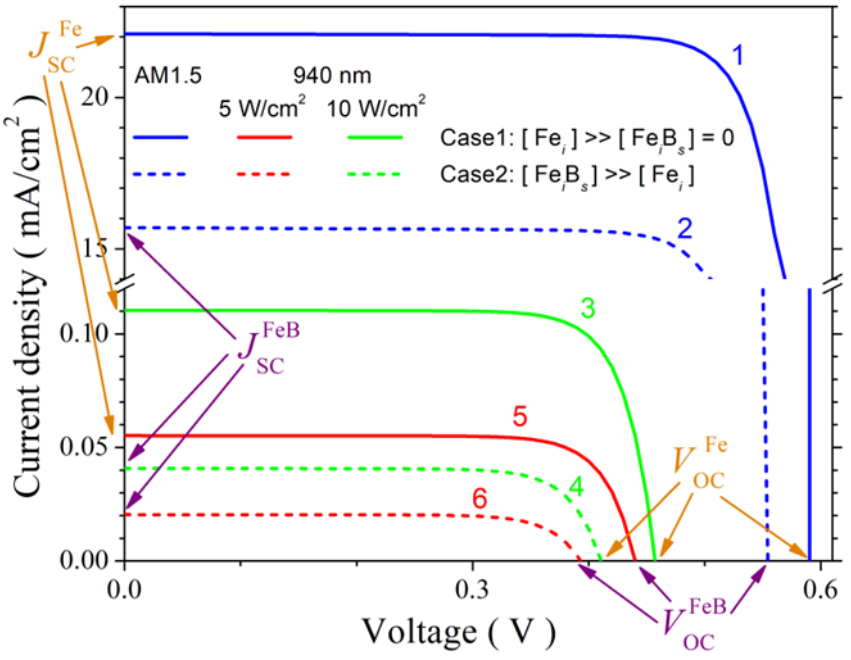

Figure 2: Typical IV characteristics, calculated for structure with d_b = 180 μ, $N_B = 10^{17}$ cm^{-3}, $N_{Fe} = 10^{14}$ cm^{-3} at T = 290 K. Illumination: AM1.5 (curves 1, 2), 940 nm 10 W/cm^2 (3, 4) and 940 nm 5 W/cm^2 (5, 6). Solid and dotted lines correspond to Case 1 and Case 2, respectively.

[18] L. Kimerling, J. Benton, Electronically controlled reactions of interstitial iron in silicon, Physica B+C 116 (1983) 297–300.
[19] C. Möller, T. Bartel, F. Gibaja, K. Lauer, Iron-boron pairing kinetics in illuminated p-type and in boron/phosphorus co-doped n-type silicon, J. Appl. Phys. 116 (2014) 024503.
[20] G. Zoth, W. Bergholz, A fast, preparation-free method to detect iron in silicon, J. Appl. Phys. 67 (1990) 6764–6771.
[21] J. Toušek, J. Toušková, A novel approach to the surface photovoltage method, Sol. Energy Mater. Sol. Cells 92 (2008) 1020–1024.
[22] S. Rein, S. W. Glunz, Electronic properties of interstitial iron and iron-boron pairs determined by means of advanced lifetime spectroscopy, J. Appl. Phys. 98 (2005) 113711.
[23] J. Schmidt, D. Macdonald, Recombination activity of iron-gallium and iron-indium pairs in silicon, J. Appl. Phys. 97 (2005) 113712.
[24] M. Goodarzi, R. A. Sinton, H. Jin, P. Zheng, W. Chen, Q. Wang, D. Macdonald, Accuracy of interstitial iron measurements on p-type multicrystalline silicon blocks by quasi-steady-state photoconductance, IEEE J. Photovolt. 7 (2017) 1216–1223.
[25] O. Olikh, V. Kostylyov, V. Vlasiuk, R. Korkishko, Y. Olikh, R. Chupryna, Features of FeB pair light-induced dissociation and repair in silicon n+-p-p+ structures under ultrasound loading, J. Appl. Phys. 130 (2021) 235703.
[26] S. Herlufsen, D. Macdonald, K. Bothe, J. Schmidt, Imaging of the interstitial iron concentration in crystalline silicon by measuring the dissociation rate of iron–boron pairs, physica status solidi (RRL) – Rapid Research Letters 6 (2012) 1–3.
[27] O. Olikh, Relationship between the ideality factor and the iron concentration in silicon solar cells, Superlattices Microstruct. 136 (2019) 106309.
[28] O. Olikh, O. Lozitsky, O. Zavhorodnii, Estimation for iron contamination in si solar cell by ideality factor: Deep neural network approach, Prog. Photovoltaics Res. Appl. 30 (2022) 648–660.
[29] R. Pässler, Dispersion-related description of temperature dependencies of band gaps in semiconductors, Phys. Rev. B 66 (2002) 085201.
[30] D. Yan, A. Cuevas, Empirical determination of the energy band gap narrowing in p$^+$ silicon heavily doped with boron, J. Appl. Phys. 116 (2014) 194505.
[31] R. Couderc, M. Amara, M. Lemiti, Reassessment of the intrinsic carrier density temperature dependence in crystalline silicon, J. Appl. Phys. 115 (2014) 093705.
[32] M. A. Green, Intrinsic concentration, effective densities of states, and effective mass in silicon, J. Appl. Phys. 67 (1990) 2944–2954.
[33] W. O'Mara, R. Herring, L. Hant, Handbook of semiconductor silicon technology, Noyes Publications, New Jersey, USA, 1990.
[34] D. Klaassen, A unified mobility model for device simulation — I. model equations and concentration dependence, Solid-State Electron. 35 (1992) 953– 959.